Available online at www.sciencedirect.com
SCIENCE DIRECT®
Journal of Power Sources 142 (2005) 81–91
JOURNAL OF POWER SOURCES
www.elsevier.com/locate/jpowsour

Kinetics, simulation and optimization of methanol steam reformer for fuel cell applications

Yongtaek Choi[a,1], Harvey G. Stenger[b,*]

[a] *Sud-Chemie Prototech Inc., Needham, MA 02494, USA*
[b] *Department of Chemical Engineering, Lehigh University, Bethlehem, PA 18015, USA*

Received 27 July 2004; accepted 20 August 2004
Available online 7 December 2004

Abstract

To evaluate reaction rates for making hydrogen from methanol, kinetic studies of methanol decomposition, methanol steam reforming, the water gas shift reaction, and CO selective oxidation have been performed. These reactions were studied in a microreactor testing unit using a commercial Cu–ZnO/Al_2O_3 catalyst for the first three reactions and Pt–Fe/γ-alumina catalyst for the last reaction. The activity tests were performed between 120 and 325 °C at atmospheric pressure with a range of feed rates and compositions.

For methanol decomposition, a simplified reaction network of five elementary reactions was proposed and parameters for all five rate expressions were obtained using non-linear least squares optimization, numerical integration of a one-dimensional PFR model, and extensive experimental data. Similar numerical analysis was carried out to obtain the rate expressions for methanol steam reaction, the water gas shift reaction, and CO selective oxidation.

Combining the three reactors with several heat exchange options, an integrated methanol reformer system was designed and simulated using MATLAB. Using this simulation, the product distribution, the effects of reactor volume and temperature, and the options of water and air injection rates were studied. Also, a series of optimization tests were conducted to give maximum hydrogen yield and/or maximum economic profit.

Keywords: Methanol decomposition; Methanol steam reforming; Water gas shift; Methanol reformer; Fuel cell; Hydrogen; Optimization

1. Introduction

The interest in hydrogen production for fuel cell applications is steadily increasing due to environmental and national security concerns. When hydrogen is used as an energy source, it produces no CO, SO_2, NO_x, VOC's and also produces no carbon dioxide. Of course, a hydrocarbon is still needed to make hydrogen for fuel cells, however a hydrogen fuel processor can be advantageous because of its energy efficiency and can lower greenhouse gases compared to the direct combustion of hydrocarbons. Therefore the use of fuel cells for transportation and electric power could reduce both toxic air pollutants and green house gas emissions.

For mobile application of fuel cells, carrying a compressed gas cylinder as the hydrogen source seems to be the most common choice today. However, there are several economical ways to make hydrogen from hydrocarbons such as gasoline, alcohols and natural gas, etc. Of the many possible hydrocarbon sources, it is not easy to choose the most promising one because of factors such as safety, economy and infrastructure. Among the various kinds of hydrocarbon choices, the advantages of high energy density, easy availability and safe handling/storage are now making methanol one of the most promising sources of hydrogen for fuel cell vehicles and small stationary power sources.

The integrated system of methanol steam reforming to produce hydrogen usually includes four reactions in three

* Corresponding author. Tel.: +1 610 758 4791; fax: +1 610 758 5057.
E-mail address: hgs0@lehigh.edu (H.G. Stenger).
[1] Tel.: 1 781 444 5188 18.

0378-7753/$ – see front matter © 2004 Elsevier B.V. All rights reserved.
doi:10.1016/j.jpowsour.2004.08.058

reactors: methanol decomposition (1) and/or methanol steam reforming (2), water gas shift reaction (3), and CO selective oxidation (4):

$$CH_3OH \leftrightarrow CO + 2H_2,\ \Delta H_{298}^{\circ} = 90.64\,kJ\,mol^{-1} \quad (1)$$

$$CH_3OH + H_2O \leftrightarrow CO_2 + 3H_2,\ \Delta H_{298}^{\circ} = 49.47\,kJ\,mol^{-1} \quad (2)$$

$$CO + H_2O \leftrightarrow CO_2 + H_2,\ \Delta H_{298}^{\circ} = -41.17\,kJ\,mol^{-1} \quad (3)$$

$$CO + (1/2)O_2 \rightarrow CO_2,\ \Delta H_{298}^{\circ} = -28.3\,kJ\,mol^{-1} \quad (4)$$

The first two reactions: methanol decomposition and methanol steam reforming on a commercial $Cu/ZnO/Al_2O_3$ catalyst were investigated in our previous paper [1]. For those reactions, a comprehensive kinetic study has been reported by Peppley et al. [2]. In their paper they derived three rate expressions, one for methanol decomposition, one for the WGS reaction and one for methanol steam reforming. They derived Langmuir–Hinshelwood rate laws from detailed surface mechanisms, resulting in 12 elementary reactions and two different active sites. Their resulting rate expressions contained numerous parameters and are overly complicated for our purposes, adding computation time with no gain in predictability. More recently there have been two other papers, which evaluate the reaction rate by an overall Arrhenius type simplified model [3–6]. However, there have been few papers that addresses both methanol decomposition, methanol steam reforming, and the known by-products.

In our previous paper [1], an eight step reaction pathway for methanol decomposition was presented, and it was shown that eight compounds are formed when methanol decomposes in the absence or scarcity of water. To design an efficient methanol reforming system, it is necessary to know the exact rates of methanol decomposition and by-product formation. In this paper we proposed that five elementary reactions are sufficient to evaluate all components in methanol decomposition. When water is added to methanol feed, the activity of catalyst increases and by-product formation decreases significantly. Also, H_2 yield increases and CO yield decreases with increasing ratio of water to methanol. Therefore, to evaluate the overall methanol reaction rate it is plausible to add the methanol steam reaction as a sixth reaction when water is present.

The water gas shift reaction is a critically important reaction to shift carbon monoxide and water to hydrogen and carbon dioxide. Although numerous studies of the reaction kinetics and mechanism for this reaction have been reported during the past decades, there are still disagreements as to what is the active site and what is the reaction mechanism [7–16]. Analyzing various proposed mechanisms, there is a distinct conflict between the "adsorptive mechanism" (5) and "regenerative mechanism" (6 + 7).

$$H_2O + CO \rightarrow CO_{(ads)} + H_2O_{(ads)} \rightarrow [int*] \rightarrow CO_{2(ads)} + H_{2(ads)} \rightarrow CO_2 + H_2 \quad (5)$$

$$H_2O + Red \rightarrow H_2 + O_x \quad (6)$$

$$CO + O_x \rightarrow CO_2 + Red \quad (7)$$

Although many rate expressions have been derived based on these mechanisms, an empirical rate expression, $r_{CO} = kP_{CO}P_{H_2O}(1-\beta)$can successfully predict the rate of the water gas shift reaction (where, the reversibility factor,$\beta = P_{H_2}P_{CO_2}/P_{CO}P_{H_2O}K_P$) [17,18].

Regardless of the reformer design and the size of the water gas shift reactor, small amounts of CO exist after hydrocarbon reforming and after the water gas shift reactor. These small amounts of CO, typically less than 1 mol%, must be removed to prevent poisoning of the fuel cell electrodes. Among the various methods to remove CO selectively, catalytic oxidation is considered as one of the most plausible and economical options. In the CO selective oxidation reaction system, in addition to the CO oxidation reaction (4), the H_2 oxidation also occurs (8)

$$H_2 + (1/2)O_2 \rightarrow H_2O,\ \Delta H^{\circ}{}_{298} = -242\,kJ\,mol^{-1} \quad (8)$$

The feed stream of a PROX reactor in a methanol fuel reformer system is composed of H_2, O_2, CO, CO_2 and H_2O. Therefore, in addition to the reactions of CO and H_2 oxidation, it is also necessary to consider the water gas shift reaction [19]. To accurately predict the concentration of all gas components in a PROX reactor, all three reactions (CO oxidation, H_2 oxidation and (reverse) water gas shift reaction) must be considered simultaneously. This three reaction system and the exact rate expressions for each reaction are important components in the optimization and control of commercial fuel reformers.

2. Experimental

For the three reactions: methanol decomposition, methanol steam reaction, and the water gas shift reaction, the $Cu/ZnO/Al_2O_3$ catalyst, a commercial catalyst manufactured by Sud-Chemie (Catalyst no.: EX-2248) was used. The catalyst used for CO selective oxidation was the Selectoxo catalyst manufactured by Engelhard ($Pt–Fe/Al_2O_3$). All catalysts were ground and sieved to a particle diameter of 200–250 μm to eliminate internal diffusion resistance. All reaction tests were performed in a standard catalyst performance evaluation unit. A stainless steel (or glass) tubular reactor, 1/2 in. in diameter and 12 in. long was used for all reaction tests. To ensure isothermal conditions along the bed length, a split

Table 1
Experimental conditions of each individual reaction

Conditions	Methanol decomposition/steam reforming	Water gas shift reaction	CO selective oxidation
Catalyst	$Cu/ZnO/Al_2O_3$	$Cu/ZnO/Al_2O_3$	$Pt–Fe/Al_2O_3$
Manufacturer	Sud-Chemie Inc.	Sud-Chemie Inc.	Engelhard
Loading amount	1.0 g	1.0 g	0.5 g + 5 g inert
Reaction temperature (°C)	120–325	120–275	80–280
Reaction pressure	Atmospheric	Atmospheric	Atmospheric
Liquid feed rate(ml h^{-1})	0.5–8	0.5–8	–
Gas feed rate (sccm)	–	70–80	160–180
GHSV (1 h^{-1})	280–4400	6000	1000–20000
Reactor	SS 316/glass tube	Glass tube	SS 316

tubular furnace was used and the temperature of the catalyst bed was measured directly by a 1/16 in. J-type thermocouple.

The reaction tests were performed at temperatures between 120 and 325 °C. For methanol reforming experiments, methanol feed rate was controlled precisely by a syringe pump, 74900 Series (Cole Palmer), from 0.5 to 8 ml h^{-1}, giving a volume of vaporized methanol at STP flow of 277–4427 cm^3 h^{-1}. In cases when water with the methanol is added, the injection rates were controlled also by the syringe pump from 0.5 to 8 ml h^{-1}. The catalyst load was between 0.25 and 1.0 g and the GHSV at reaction temperature was controlled between 1000 and 10,000 h^{-1}.

For the water gas shift experiments, the feed gas stream was a 1:2 mixture of CO and hydrogen to simulate the conditions exiting a methanol reforming unit. For the PROX experiments, the feed gas stream contained 62–72% H_2, 0.5–5.0% O_2, 2–17% N_2, 0.5–3.0% CO, and 20–24% CO_2 (dry basis). The catalyst load was 1.0 g for the WGS and 0.5 g for PROX and the GHSV at reaction temperature was controlled between 1000 and 20,000 h^{-1}. All the reaction runs were performed under atmospheric pressure. The experimental conditions of this reaction system are summarized in Table 1.

The effluent of the reactor was maintained at 120 °C with heating tapes to avoid liquid condensation and connected directly to a CARLE Series S gas chromatograph, which uses a Hydrogen Transfer System (Pd membrane) for hydrogen analysis. This is a specially designed GC with dual TCD using two different carrier gases: helium and nitrogen. Helium is the preferred carrier gas for all components except hydrogen while nitrogen is the proper carrier gas for hydrogen. Two columns: Alltech Chemisorb 107 (80–100 mesh, 6 ft × 1/8 in.) and Supelco Carboxen 1000 (60–80 mesh, 15 ft × 1/8 in.) were connected in series to analyze the condensible and light gas components. Eight components: water, methanol, dimethyl ether, methyl formate, H_2, CO, CH_4, CO_2 were measured during each test run. Material balances on carbon were calculated to verify measurement accuracy. For CO selective oxidation, the GC chamber was maintained at a constant temperature of 50 °C to separate N_2 and O_2 properly. Five components H_2, O_2, N_2, CO and CO_2 were measured during each test run. Material balances on carbon were calculated to verify measurement accuracy, and for all runs reported here were within 3% of closure.

3. Results

3.1. Methanol decomposition and methanol steam reaction

Before running the steam-methanol reaction, tests of methanol decomposition were conducted using pure methanol in the absence of water. When methanol decomposes over the $Cu/ZnO/Al_2O_3$ catalyst it produces hydrogen and CO as main components and several by-products such as methyl formate, carbon dioxide, dimethyl ether and methane. Fig. 1 shows a product distribution of all the components leaving the reactor as a function of temperature at a space velocity of 4400 h^{-1}. Methyl formate, which was a main by-product when methanol is not fully decomposed, reached its maximum concentration of about10 mol% at temperatures between 285 and 300 °C. The other by-products, CO_2, dimethyl ether and methane were formed between 1 and 3%. For the kinetic study of methanol decomposition, 43 runs were made at five different space velocities. All of these data points are shown in Fig. 2.

When water is added to the feed, methanol decomposes more rapidly at lower temperatures and shows a different pattern of product distribution. Fig. 3 shows the conversion of

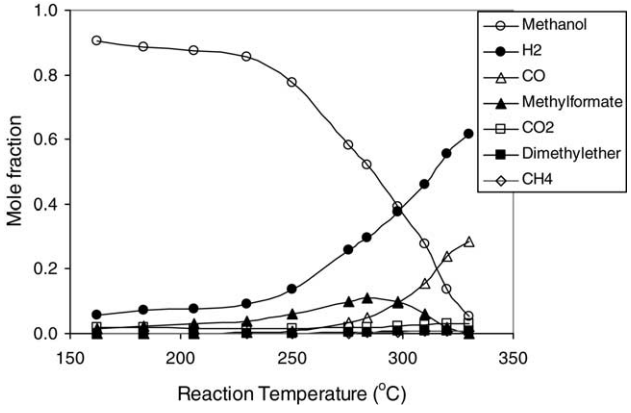

Fig. 1. Methanol decomposition in the absence of water: mole fraction of the products at the reactor outlet (methanol, hydrogen, carbon monoxide, methyl formate, carbon dioxide, dimethyl ether, methane, catalyst loading: 1.0 g, GHSV: 4400 h^{-1}).

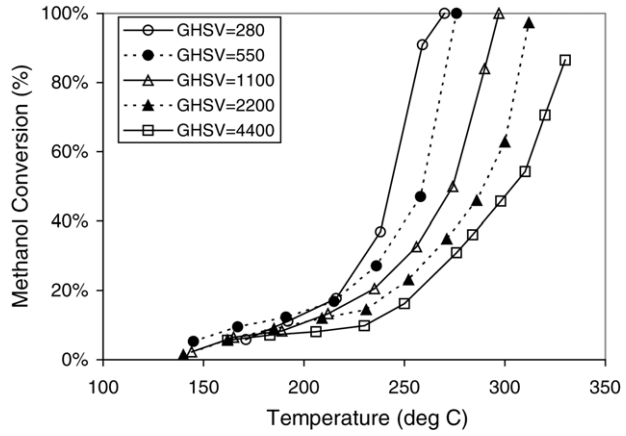

Fig. 2. Conversion of methanol with various space velocities in the absence of water as a function of reaction temperature (1.0 g of $Cu/ZnO/Al_2O_3$ catalyst, methanol feed: Laboratory Grade, GHSV: 280–4400 h^{-1}).

methanol versus reaction temperature when water is added to the methanol feed. Complete methanol conversion occurs near 250 °C when water addition is more than 30 wt.% of the feed (43 mol%). Another effect of water addition is the reduction of all the observed by-products: dimethyl ether (DME), methyl formate and methane. Methyl formate, the main by-product for methanol-only decomposition was reduced significantly as water was added and no methyl formate was detected when the feed contains greater than 43 mol% water. Also there was no DME formation when the feed had more than 24 mol% water and no methane was detected after a feed of 8.6 mol% of water.

3.2. Water gas shift reaction

Fig. 4 shows the water gas shift conversion of carbon monoxide with various H_2O/CO ratios in the temperature range of 120–250 °C. As a consequence of equilibrium, the

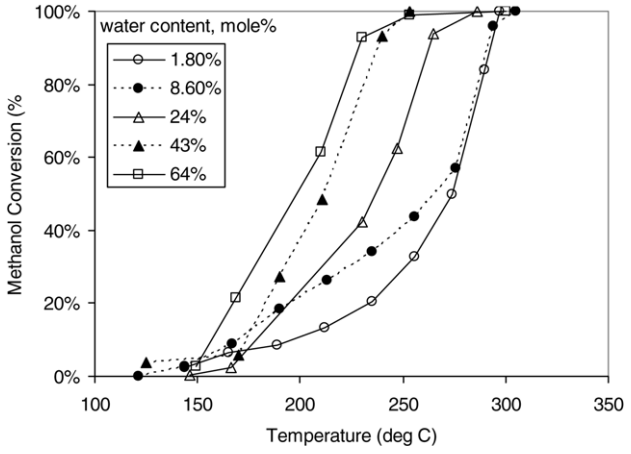

Fig. 3. Methanol conversion in methanol steam reaction as a function of reaction temperature (water content in feed = 1.8, 8.6, 24, 43, 64 mol%, catalyst loading = 1.0 g, GHSV = 1100 h^{-1}).

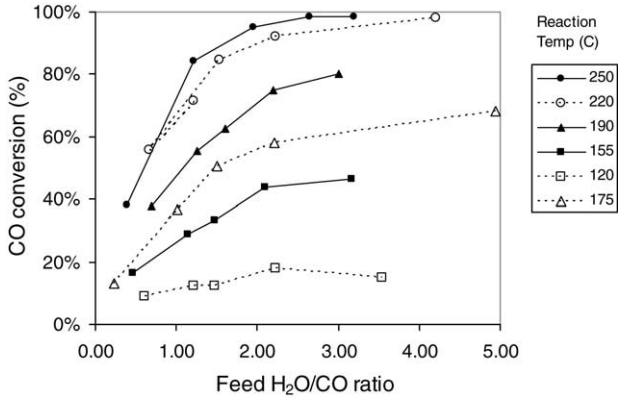

Fig. 4. Water gas shift reaction: CO conversion vs. feed H_2O/CO ratio (reaction temperature: 175–250 °C, catalyst loading: 1.0 g, pressure: 1 atm, GHSV: 6100 1 h^{-1}).

conversion of CO consistently increases with the H_2O/CO ratio at constant temperature. For example a 1:1 molar feed ratio and 220 °C, the conversion reaches 70% while the equilibrium conversion is calculated to be 87%.

3.3. CO oxidation

Fig. 5 shows a plot of CO oxidation conversion at various O_2/CO feed ratios as a function of reaction temperature for the Selectoxo catalyst. As shown in this figure, the conversion of CO increases at high O_2/CO ratios and low CO concentrations. When the O_2/CO ratio was 2.0, the CO conversion was more than 95% even under 200 °C. In the three cases where the O_2/CO mole ratio is near 1.0, lower CO concentrations gave higher CO conversions. All data points in this figure were used to determine the rate expressions of three reactions in the PROX system.

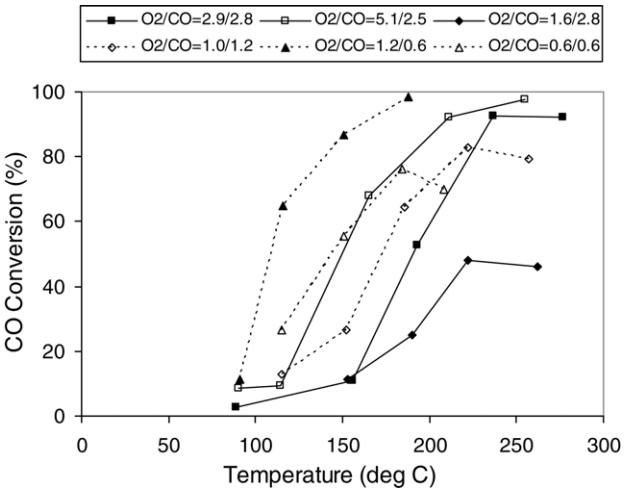

Fig. 5. Conversion for CO selective oxidation with various O_2/CO ratio as a function of reaction temperature: 0.5 g of Selectoxo (Pt–Fe/γ-alumina) catalyst, flow rate: 167 sccm, H_2: 64–75 mol%, O_2/CO in mol%, 1 atm, no water addition.

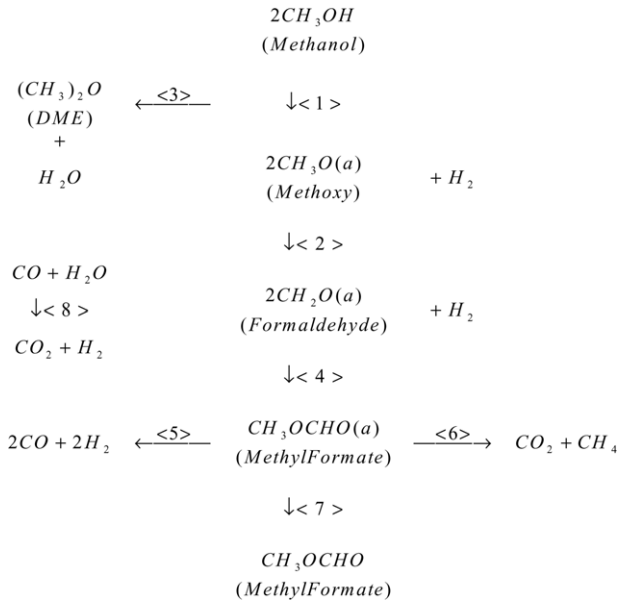

Fig. 6. Schematic diagram of simplified eight steps reaction mechanism of methanol decomposition.

3.4. Kinetic studies and analysis

3.4.1. Methanol decomposition

The reaction mechanism of methanol decomposition and methanol steam reforming was studied in a previous paper [1], however a complete kinetic model was not presented there. Based on the reaction mechanism shown in Fig. 6 an eight step reaction model of methanol decomposition can be written for the five elementary reactions. The rate expressions assumed for each reaction are listed in Table 2.

The constants k_1 to k_5 of Table 2 are assumed to be functions of temperature in the expression of $A_i \exp(E_i/RT)$. The 10 unknown parameters were found using the following steps. (1) A_2 and E_2 were determined from the DME and MeOH data alone, using a material balance on DME. (2) A_4, A_5, E_4 and E_5 were then determined using MF and methane balances. (3) A_3, E_3 were determined from the WGS experiments independently. (4) A_1 and E_1 were determined using a material balance on MeOH. For step (1) and (2) the expression in Eq. (9) was minimized.

$$\text{minimize}\left\{F = \sum_{i=1}^{N} (pe_i - pc_i)^2\right\} \tag{9}$$

Table 3
Activation energy and frequency factors for methanol decomposition

Reaction	Activation energy (kJ mol^{-1})	Frequency factor (mol g_{cat}^{-1} s^{-1} atm*)
$CH_3OH \rightarrow CO + 2H_2$	91.8	5854
$2CH_3OH \rightarrow CH_3OCH_3 + H_2O$	88.9	125
$CO + H_2O \rightarrow CO_2 + H_2$	43.7	17.973
$2CH_3OH \rightarrow CH_3OCHO + 2H_2$	82.2	1650
$CH_3OCHO \rightarrow CO_2 + CH_4$	45.6	1.174

* For second order reaction, the unit is (mol g_{cat}^{-1} s^{-1} atm^{-2}).

For steps (3) and (4) the expression in Eq. (10) was minimized.

$$\text{minimize}\left\{f = \sum_{i=1}^{N} (X_{e,i} - X_{c,i})^2\right\} \tag{10}$$

where, F or f is the objective function of optimization for minimizing, i the number of data points ($i = 43$ for DME, MF, and MD, $i = 30$ for WGS); p_e the experimental partial pressure of a component at the reactor outlet (atm); p_c the calculated partial pressure of a component at the reactor outlet (atm); X_e the experimental conversion of a component; X_d the calculated conversion of a component.

The exit partial pressure of each component was determined by numerically integrating a one-dimensional isothermal PFR model. For example, the MeOH balance was written as follows:

$$\frac{dn_{CH_3OH}}{dW} = -A_1 \exp\left(\frac{-E_1}{RT}\right)\left(P_{CH_3OH} - \frac{P_{H_2}^2 P_{CO}}{K_{p,md}}\right) - A_2 \exp\left(\frac{-E_2}{RT}\right) P_{CH_3OH}^2 - A_4 \exp\left(\frac{-E_4}{RT}\right) P_{CH_3OH}^2 \tag{11}$$

where, nCH$_3$OH is the molar flow rate of methanol, W the catalyst weight (g); A_i the frequency factor; E_i the activation energy; P_i the partial pressure of the component i (atm); $K_{p,mp}$ the equilibrium constants of methanol decomposition.

MATLAB subroutine functions "ODE23" and "Lsqnonlin" were used for numerical integration and optimization. A summary of the rate parameters is shown in Table 3. The quality of the fit for the overall model is demonstrated in Fig. 7 by comparing the observed and calculated rate of ex-

Table 2
Reactions and rate expressions for methanol decomposition systems

Reaction	Formula	Rate law
Methanol decomposition	$CH_3OH \leftrightarrow CO + 2H_2$	$-r_1 = k_1(P_{CH_3OH} - K^{-1} P_{H_2}^2 P_{CO})$
DME formation	$2CH_3OH \rightarrow CH_3OCH_3 + H_2O$	$-r_2 = k_2(P_{CH_3OH})^2$
WGS reaction	$CO + H_2O \leftrightarrow CO_2 + H_2$	$-r_3 = k_3(P_{CO} P_{H_2O} - K^{-1} P_{H_2} P_{CO_2})$
MF formation	$2CH_3OH \rightarrow CH_3OCHO + 2H_2$	$-r_4 = k_4(P_{CH_3OH})^2$
Methane formation	$CH_3OCHO \rightarrow CO_2 + CH_4$	$-r_5 = k_5 P_{MF}$

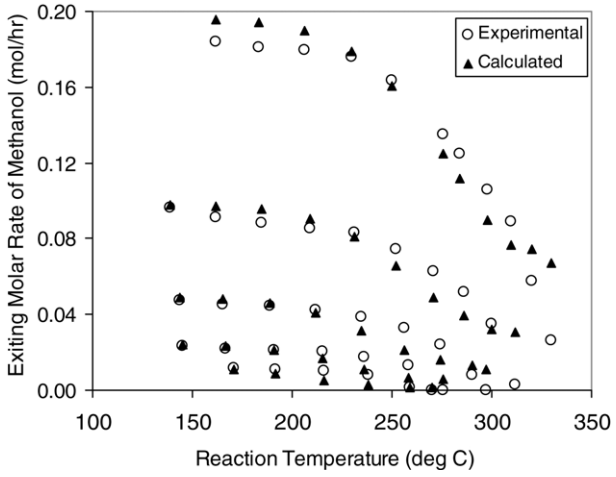

Fig. 7. Comparison of experimental data with calculated value for the rate of methanol exiting reactor (temperature: 175–250 °C, catalyst loading: 1.0 g, pressure: 1 atm).

iting methanol for all experiments. Although some data is slightly skewed, the overall quality is quite good.

A detailed confirmation of the accuracy of the methanol decomposition kinetic model is accomplished by comparing the calculated and experimental exiting molar rates of all the reactants and products. Figs. 8 and 9 show the fit of DME and MF concentrations by the model, and indicate a high degree accuracy.

3.4.2. Water gas shift reaction

Fig. 10 shows the comparison of experimental exit flow rate of CO with the calculated values obtained from kinetics in the water gas shift reaction. The WGS kinetics were found independent of the methanol decomposition reaction. An empirical rate expression was used: $r_{CO} = kP_{CO}P_{H_2O}(1-\beta)$, where β is the reversibility factor of the reaction defined as $\beta = P_{CO_2}P_{H_2}/P_{H_2O}P_{CO}K_p$ and K_p is the equilibrium constant. The values of A_2 and E_2 are shown in Table 3.

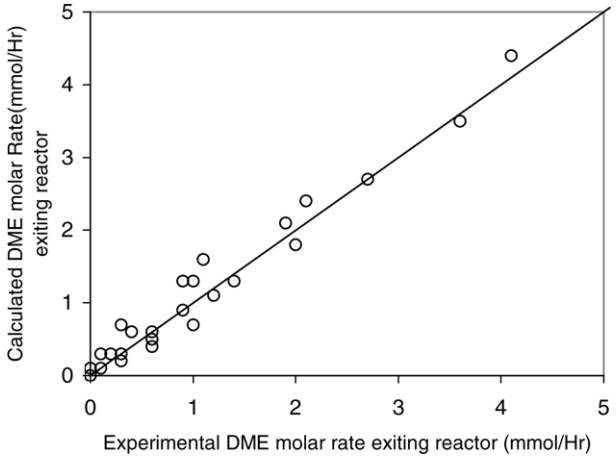

Fig. 8. Comparison of experimental rate with calculated value for (temperature: 20–325 °C, catalyst loading: 1.0 g, pressure: 1 atm).

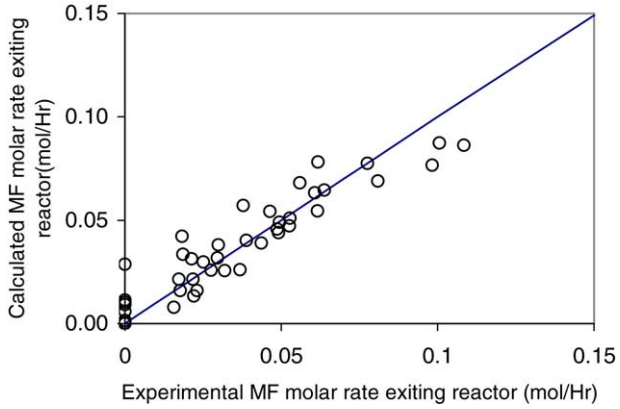

Fig. 9. Comparison of experimental data with calculated value for methyl formate (temperature: 120–325 °C, catalyst loading: 1.0 g, pressure: 1 atm).

Attempting to predict the experimental data for the methanol steam reforming tests using only the five reactions of Table 2, which excluded the methanol steam reaction ($CH_3OH + H_2O \leftrightarrow CO_2 + 3H_2$) was not successful. However, when a sixth reaction with the rate $-r_6 = k_6(P_{CH_3OH}P_{H_2O})$ is added, the model fit of the data greatly improved. Therefore, a sixth reaction was added to simulate the reaction of methanol steam reforming. The rate expression for this sixth reaction was found to be:

$$r_6 = 2.67 \times 10^6 \exp\left(\frac{-70358}{RT}\right)(P_{CH_3OH}P_{H_2O}) \quad (E_6 = \mathrm{J\,mol^{-1}},\quad P = \mathrm{atm}) \quad (12)$$

3.4.3. PROX reaction

For the CO PROX system, a reaction model in which three reactions (CO oxidation, H_2 oxidation and the water gas shift reaction) occur simultaneously was chosen and the empirical rate expressions derived from the numerical analysis are as

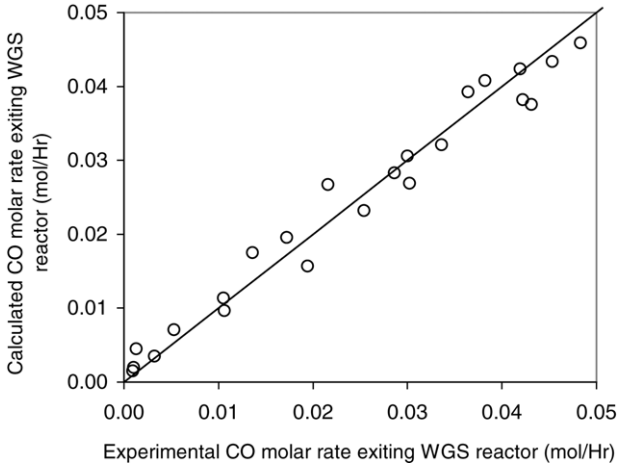

Fig. 10. Comparison of experimental data with calculated value for the water gas shift reaction (temperature: 175–250 °C, catalyst loading: 1.0 g, pressure: 1 atm).

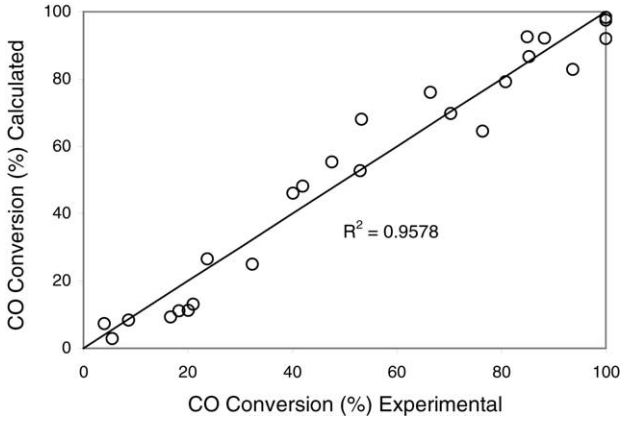

Fig. 11. Comparison of experimental data with calculated values for CO selective oxidation. A 0.5 g of Selectoxo (Pt–Fe/γ-alumina) catalyst, flow rate: 167 sccm, H_2: 62–72 mol%, O_2/CO: 0.5–2.0, reaction temperature: 100–300 °C, pressure: 1 atm, no water addition.

follows:

$$-r_1 = 3.528 \times 10^2 \exp\left(\frac{-33092}{RT}\right) P_{O_2}^{0.5} P_{CO}^{-0.1} \quad (E_1 = \mathrm{J\,mol^{-1}}, \quad P = \mathrm{atm}) \quad (13)$$

$$-r_2 = 2.053 \times 10 \exp\left(\frac{-18742}{RT}\right) P_{O_2}^{0.5} \quad (E_2 = \mathrm{J\,mol^{-1}}, \quad P = \mathrm{atm}) \quad (14)$$

$$-r_3 = 4.402 \times 10^3 \exp\frac{-34104}{RT}\left(P_{CO} P_{H_2O} - \frac{P_{CO_2} P_{H_2}}{K_P}\right) \quad (E_3 = \mathrm{J\,mol^{-1}}, \quad P = \mathrm{atm}) \quad (15)$$

The quality of the fit is shown in Fig. 11 by comparing the observed and calculated CO conversion and selectivity for all the experiments. As shown in the figure, the calculated values show good agreement with the experiments.

4. Simulation and optimization

4.1. Combined reactions and integrated system

The integrated system of methanol steam reforming includes three reactors: reformer, WGS reactor, and PROX reactor. In this reactor system, water can be added to any or all three reactors and a variable amount of air must be added to the PROX reactor. Also an energy balance must be satisfied for each reactor that includes heats of reaction, latent heats, sensible heats, and heat transfer. Fig. 12 shows the simplified process flow diagram of the methanol reformer system used for process simulation and optimization. In this integrated system, three reactors, three mixing points, three heat exchangers, 10 reactions, and 10 components of reactants and products are considered. Based on the reaction kinetics obtained above, a process simulation program was coded

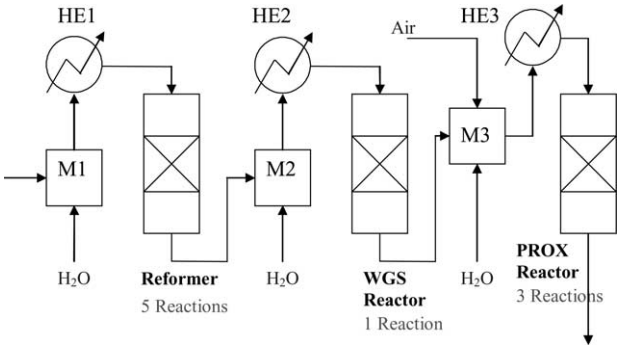

Fig. 12. Process flow diagram for methanol reformer optimization HE1, HE2, and HE3 are the heat exchangers and M1, M2, and M3 are mixing points.

using MATLAB. The simulation assumed one-dimensional PFR models and used the subroutine functions "ODE23" for integration.

Fig. 13 shows the composition profile in the simulated methanol steam reformer operated at a point to produce enough H_2 for a 1 kW fuel cell. In this simulation, the feed rate was 10 mol h^{-1} (methanol + water) and the water content was 23.8 mol%, the reactor temperature was 250 °C and the reactor contained 250 g of $Cu/ZnO/Al_2O_3$ catalyst. When comparing the simulation result with the corresponding experimental data, all of the exiting flow rates are well matched with the experimental values

4.2. The effects of reformer reactor volume and temperature

Fig. 14 is a contour plot of catalyst weight in the reformer, reformer temperature, and H_2 yield per unit methanol feed, for the three reactor integrated system. For this simulation the process variables of temperatures and catalyst loadings of WGS and PROX reactor, amount of water addition, and the

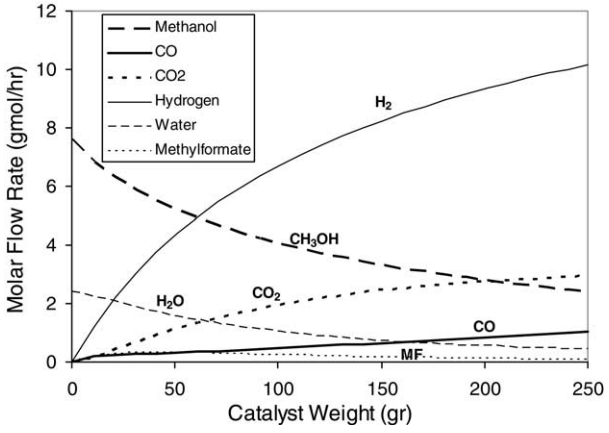

Fig. 13. Simulation of methanol steam reaction: product distribution through the reactor bed (feed rate: 10 gmol h^{-1} of methanol, water content: 23.8 mol%, inlet temperature: 250 °C, catalyst: 250 g, isothermal).

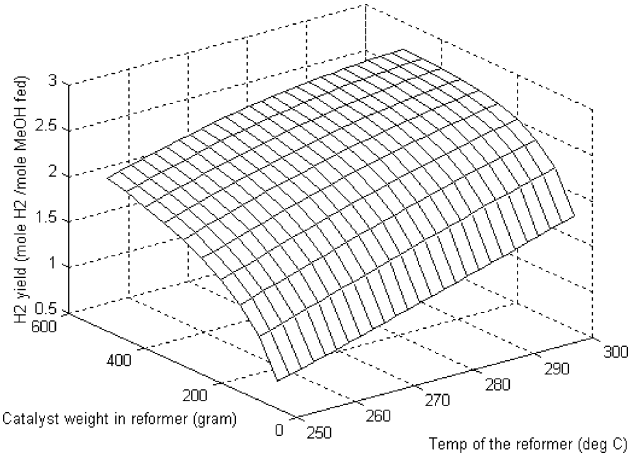

Fig. 14. Simulation of integrated system of methanol fuel reformer: effect of reformer volume and temperature on hydrogen yield (reactor temperatures – WGS: 220 °C, PROX: 200 °C; catalyst loading – WGS: 500 g, PROX: 40 g; water addition – MD: 10 mol h^{-1}, WGS: 5 mol h^{-1}, PROX: 3 mol h^{-1}, O_2/CO ratio: 1.1).

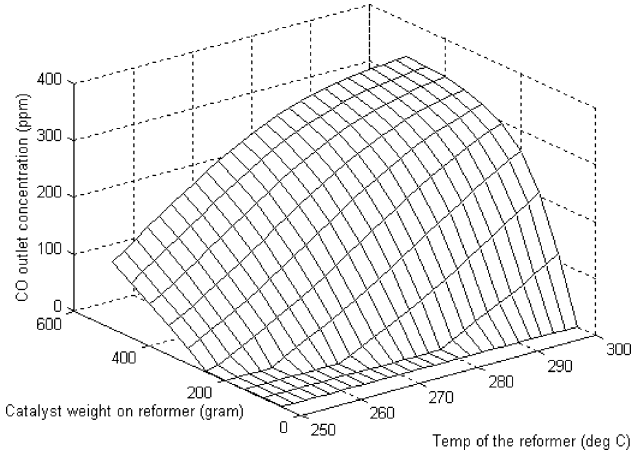

Fig. 15. Simulation of integrated system of methanol fuel reformer: effect of reformer volume and temperature on CO outlet concentration (reactor temperatures – WGS: 220 °C, PROX: 200 °C; catalyst loadings – WGS: 500 g, PROX: 40 g; water addition – MD: 10 mol h^{-1}, WGS: 5 mol h^{-1}, PROX: 3 mol h^{-1}, O_2/CO ratio: 1.1).

PROX O_2/CO ratio were fixed at conditions shown in Table 4. As shown in Fig. 14, the hydrogen yield increases expectedly with increasing reformer catalyst weight and increasing reformer temperature. However, the CO concentration exiting the integrated system (exit of PROX reactor) also increases with increasing temperature and reformer catalyst volume, as shown in Fig. 15. To meet a specific CO tolerance specification, for example 30 ppm, it is expected that an optimum condition of reformer temperature and volume may exist.

4.3. The effects of water addition

To produce hydrogen from methanol or hydrocarbon sources, the addition of water is always advantageous. But the location and amount of water to add is not as obvious. To add water to the reformer system, three locations are possible: the inlet of the reformer with the methanol feed, the inlet of the WGS reactor, and the inlet of PROX reactor. Fig. 16 is a contour plot of hydrogen yield and Fig. 17 is the exiting CO concentration versus water addition rates to the reformer and the WGS reactor. For these plots, the variables of reactor volume, temperature, and O_2/CO ratio are fixed at the conditions in Table 4. These figures show that water is advantageous for both hydrogen yield and CO outlet concentration. Therefore, the proper amount of water should be determined after considering the energy penalty imposed by the water.

Table 4
Base conditions of the variables for simulation and optimization

Types	Description	Unit	Conditions
Reactor size	Methanol reformer	g catalyst	250
	Water gas shift reactor	g catalyst	500
	PROX reactor	g catalyst	40
Reactor Temperature	Methanol reformer	°C	300
	Water gas shift reactor	°C	220
	PROX reactor	°C	200
Water Injection	Methanol reformer	mol h^{-1}	10
	Water gas shift reactor	mol h^{-1}	5
	PROX reactor	mol h^{-1}	3
O_2/CO ratio	PROX reactor	–	1.1

4.4. Reformer optimization and economic analysis

Critical to the system design is finding the optimum reactor sizes and operating conditions of temperature, amount of water added to each reactor, and the air to CO ratio to the PROX reactor. For example, a bigger WGS reactor results in a smaller PROX reactor, which results in an important design trade off between the size of the WGS reactor and the size of the selective oxidation reactor.

To make a compact and efficient fuel reformer, many variables must be optimized simultaneously. Based on the kinet-

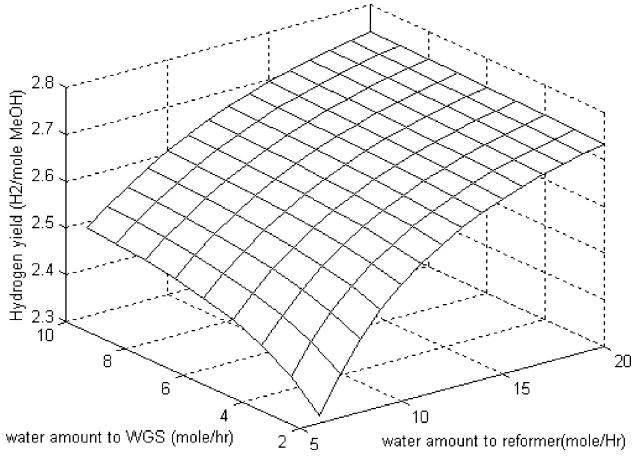

Fig. 16. Simulation of integrated system of methanol fuel reformer: effect of water addition on hydrogen yield (reactor temperatures – MD: 300 °C, WGS: 220 °C, PROX: 200 °C; catalyst loadings – MD: 250 g, WGS: 500 g, PROX: 40 g; water addition – PROX: 3 mol h^{-1}, O_2/CO ratio: 1.1).

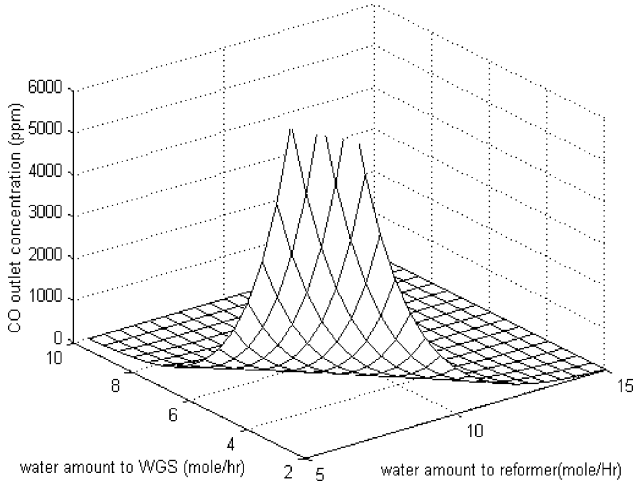

Fig. 17. Simulation of integrated system of methanol fuel reformer: effect of water addition on product CO concentration (reactor temperatures – MD: 300 °C, WGS: 220 °C, PROX: 200 °C; catalyst loadings – MD: 250 g, WGS: 500 g, PROX: 40 g; water addition – PROX: 3 mol h^{-1}, O_2/CO ratio: 1.1).

ics of the reactions and our simulation program, a number of optimization tests for the integrated reformer system were performed. For this optimization, an approximate economic profit was used as the objective function. Profit is defined as the difference between hydrogen revenue and the fixed plus operating cost of production. In this optimization the temperatures of the reactions were limited from 100 to 350 °C to avoid condensing water and thermal degrading of the catalysts. Also the total rates of water addition were limited to 20 mol h^{-1}, which is imposed by the humidity limits of the fuel cell.

For hydrogen revenue, the current prices of cylinder supplied hydrogen were used. The prices are summarized in Table 5. Depending on purity, the hydrogen price varies from 0.05 to 1.12 $ $gmol^{-1}$. A hydrogen purity factor was derived from this data using the relation between H_2 purity and prices. According to the CO outlet concentration, the purity factor (pufc) is expressed as follows:

$$\text{pufc} = 1.1983 \exp(-0.0052\text{CO ppm}) \quad (16)$$

The revenue from producing hydrogen was calculated by multiplying the hydrogen price, times the purity factor, times the hours of reformer operation times the hydrogen flow rate.

The reactor costs were determined from the mass of catalyst times a cost factor of 1 for the WGS and MSR reactors and 5 for the PROX reactor. Energy costs for heating were calculated assuming methanol is combusted to provide the necessary heat and that cooling was free. These are optimistic, but a place to start our analysis. Factors related to hydrogen price, reactor costs, and energy costs are summarized in the Table 6. To maximize the profit function, the optimization program minimized (cost − revenue) using the "fmincon" function in MATLAB and the subroutines previously discussed.

Table 5
Hydrogen price

Supplier	Grade	H_2 purity	Price ($ kg^{-1})
Scott specialty gases*	Research	99.9999	560
	Ultra-high purity	99.999	150
	Pre-purified	99.99	84
Airgas	High purity	99.9	44
	Industrial	99	25

* Based on cylinder size K: 262 $ft^{3.}$

The methanol decomposition reaction is endothermic and is favored at high temperatures while the water gas shift reaction is favored at low temperatures. However the reforming reactor must not run too hot to prevent catalyst deactivation and high energy costs. Also the water gas shift reactor has an optimum temperature because the rate of the reaction is kinetically slow at low temperatures but favored thermodynamically. CO selective oxidation is strongly exothermic with little or no thermodynamic limitations, however if temperatures are too high the reverse water gas shift reaction rate increases in the PROX reactor and produces CO rather than consuming it.

To test the optimization of the profit function it was easiest to fix several of the 10 operating variables in Table 6 and search for optimum values for the remaining variables. The feed rates and reactor sizes (except the reforming reactor) were fixed at those values in Table 6 and the reactor temperatures that gave the highest profit were calculated and are plotted versus reformer size in Fig. 18. As shown in this figure, the operating temperature of the reformer is optimum in the range of 300–350 °C while the optimum temperatures of WGS and PROX reactor are very constant at 220 and 250 °C, respectively.

Water and feed rates were also tested for optimum behavior. In Fig. 19, optimum water addition rates were obtained to maximize profit as a function of the size of the methanol steam reformer. All other values, size of reactors, temperatures of reactors and O_2/CO in PROX were fixed at those values in Table 6. As shown in Fig. 19, there exist op-

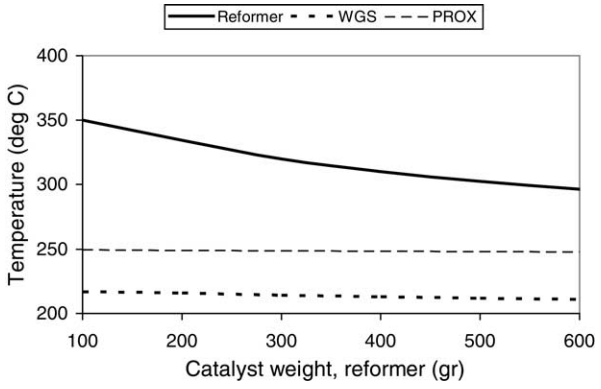

Fig. 18. Optimum operating temperatures of the reformer, WGS reactor, and PROX reactors with regard to the size of the reformer (catalyst loading – WGS: 300 g, PROX: 50 g; water addition – MD: 10 mol h^{-1}, WGS: 5 mol h^{-1}, PROX: 3 mol h^{-1}, O_2/CO ratio: 1.1).

Table 6
Fixed conditions of the variables in the optimization

Symbol	Description	Unit	Values
h2price	Hydrogen price (99.995)	$\$\,gmol^{-1}$	0.25
pufc	Purity factor	–	$1.1983\exp(-0.0052CO\,ppm)$
rx1cf	Cost for methanol steam reformer	$\$\,g_{cat}{}^{-1}$	1
rx2cf	Cost for water gas shift reactor	$\$\,g_{cat}{}^{-1}$	1
rx3cf	Cost for PROX reactor	$\$\,g_{cat}{}^{-1}$	5
qc1	To heat feed to reformer temperature	$\$\,{}^{\circ}C^{-1}\,gmol^{-1}$	1.41×10^{-6}*
qc2	To supply reaction heat for MD	$\$\,kJ^{-1}$	1.72×10^{-5}**
qc3	To cool reformate to WGS temp.	Free	–
qc4	To remove reaction heat of WGS	Free	–
qc5	To cool reformate to PROX temp.	Free	–
qc6	To remove reaction heat of PROX	Free	–

* Based on methanol price, $0.64\,\$\,gal^{-1}$ and heat of combustion, $397\,kJ\,mol^{-1}$.
** Based on the heat capacity of methanol at 20 °C, $82.0\,J\,mol^{-1}\,K^{-1}$.

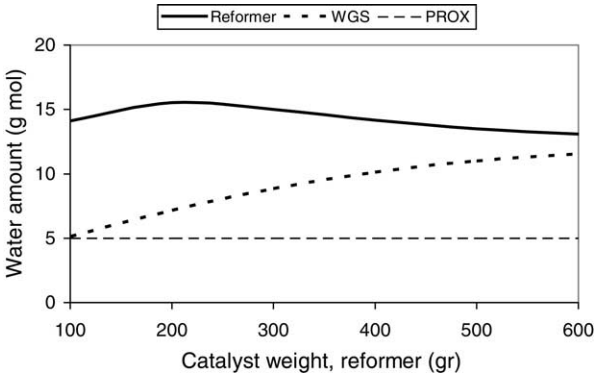

Fig. 19. Optimized water addition rates to reformer WGS reactor, and PROX reactors with regard to the size of the reformer (catalyst loading – WGS: 300 g, PROX: 50 g; water addition – MD: $10\,mol\,h^{-1}$, WGS: $5\,mol\,h^{-1}$, PROX: $3\,mol\,h^{-1}$, O_2/CO ratio: 1.1).

timum levels of water addition for methanol steam reformer ($13–15.5\,gmol\,h^{-1}$) and WGS reactor ($5.2–11.5\,gmol\,h^{-1}$) while a lesser effect of water addition exists for the PROX reactor.

5. Conclusion

The reaction kinetics for the six reactions in a methanol steam reformer, the one reaction in the water gas shift reactor, and the three reactions in a CO selective oxidation reactor were measured and all 10 rate expressions were obtained from a large set of experimental data from commercial $Cu/ZnO/Al_2O_3$ and Pt–Fe catalysts. Applying these empirical relationships in simple plug flow reactor models, it is possible to gain insights into the design and operation of the reformer, the WGS, and the PROX reactors, as well as the integrated system. Using these rate expressions the system was simulated and optimized to maximize profit.

The simulation and optimization results show that the performance of the integrated system is greatly affected by the size of the reformer and not sensitive to the temperature of the WGS reactor or PROX reactor. For best performance, the water gas shift reactor should be operated in the range of 220 °C regardless of other process conditions. For the CO oxidation reactor, the operating temperature and reactor size have less impact on the performance of the reactor, but O_2/CO ratio should be maintained higher than stoichiometry to avoid high CO concentrations in the final product. Although our optimization efforts are simplistic and brief, their usefulness is significant. The results of this study are expected to be a critical part of the overall design, optimization and control of fuel reformer systems.

Acknowledgements

The authors thank the APERG sponsorship from Air and Waste Management Association, Sud Chemie Inc. and Engelhard Corporation for the catalyst.

References

[1] Y. Choi, H.G. Stenger, Appl. Catal. B: Environ. 38 (2002) 251–361.
[2] B.A. Peppley, et al., Appl. Catal. A: Gen. 179 (1999) 21–49.
[3] J. Agrell, H. Birgersson, M. Boutonnet, J. Power Sources 106 (2002) 249–257.
[4] K. Takeda, A. Baba, Y. Hishinuma, T. Chikahisa, JSAE Rev. 23 (2002) 183–188.
[5] Konard Geissler, et al., Phys. Chem. Chem. Phys. 3 (2001) 289–293.
[6] P. Mizsey, E. Newson, T. Truong, P. Hottinger, Appl. Catal. A: Gen. 213 (2001) 233–237.
[7] T.M. Yureva, Kinet. Katal. 10 (1969) 862.
[8] C. Rhodes, G.J. Hutchings, A.M. Ward, Catal. Today 23 (1995) 43–58.
[9] T. Shido, Y. Iwasawa, J. Catal. 129 (1991) 343–345.
[10] G.J. Millar, C.H. Rochester, K.C. Waugh, J. Catal. 142 (1993) 263–273.
[11] G. Shchibrya, N. Morozov, M. Temkin, Kinet. Catal., USSR 6 (1965) 1010.
[12] O. Jakdetchai, T. Nakajima, J. Mol. Struct. (Theorem) 619 (2002) 51–58.
[13] C.V. Ovesen, et al., J. Catal. 158 (1996) 170–180.

[14] G.F. Froment, K.B. Bischoff, Chemical Reactor Analysis and Design, 2nd ed., Wiley, 1990.
[15] J.S. Cambell, Ind. Eng. Chem. Proc. Res. Dev. 9 (1970) 588.
[16] N. Amadeo, M. Laborde, Int. J. Hydrogen Energy 20 (12) (1995) 949–956.
[17] R.L. Keiski, O. Desponds, Y.F. Chang, G.A. Somorjai, Appl. Catal. A 101 (1993) 317–338.
[18] Yongtaek Choi, Harvey Stenger, J. Power Sources 124 (2) (2003) 432–439.
[19] Y. Choi, H. Stenger, J. Power Sources 129 (2) (2004) 246–254.